High-field hole transport in silicon nanowires

A. Verma,[1,a] A. K. Buin,[2] and M. P. Anantram[3]
[1]*Department of Electrical Engineering and Computer Science, Texas A&M University-Kingsville, Kingsville, Texas 78363, USA*
[2]*Département de Chimie, Université de Montréal, Montréal, Québec, H3T 1J4 Canada*
[3]*Department of Electrical Engineering, University of Washington, Seattle, Washington 98195, USA*

(Received 19 May 2009; accepted 22 October 2009; published online 10 December 2009)

We report on ensemble Monte Carlo hole transport simulations for small diameter silicon nanowires. The basis for the simulations is provided by band structure calculations using $sp^3d^5s^*$ tight-binding scheme. Principal scattering mechanisms considered are hole-bulk acoustic and optical phonon interactions. Both steady-state and transient hole transport characteristics are explored. For the silicon nanowires considered, the steady-state average hole drift velocity saturates due to optical phonon scattering. Acoustic and intersubband scattering mechanisms strongly prevent an oscillation in the hole velocity in the transient regime. Room temperature hole mean free path for the different silicon nanowires considered is evaluated to be less than 10 nm at various electric fields. © *2009 American Institute of Physics*. [doi:10.1063/1.3264629]

I. INTRODUCTION

Over the last decade, silicon nanowires (SiNWs) have caught significant attention as basic building blocks for future nanoscale electronic and sensor devices.[1–3] Within this context our recent theoretical work has suggested that low-field charge carrier mobility in small diameter [110] axially aligned SiNWs may be significantly greater than in other SiNWs,[4] with low-field hole mobility exceeding bulk silicon hole mobility for some of the SiNWs. This enhancement in hole mobility is further supported by experimental results.[5] These results strongly suggest the need for a further exploration of hole transport in [110] SiNWs, specifically an understanding of the behavior of hole transport at high electric fields, and further comparison with other SiNWs with different crystallographic orientations.

In this paper we report on an ensemble Monte Carlo (EMC) study of hole transport in small diameter SiNWs[6] in both steady-state and transient regimes. EMC simulation is a particularly useful and flexible tool to investigate steady-state and transient charge carrier transport under relatively moderate and high electric fields in semiconductors.[7] Section II of this paper provides a brief description of the band structure and scattering rate models utilized in this work. A more detailed discussion of these models may be found in earlier work.[4] EMC simulations are performed at various electric fields and temperatures. The results are presented and discussed in Sec. III. Conclusions are drawn in Sec. IV.

II. MODEL DESCRIPTION

In this work freestanding SiNWs with hexagonal cross-section shape are considered, where the diameter of a SiNW signifies the diameter of the smallest possible circle that fully contains the cross section. Silicon dangling bonds on the surface are passivated with hydrogen atoms. The band structure of the SiNWs is obtained using a $sp^3d^5s^*$ tight-binding (TB) scheme.[4] This parametrization scheme has been found to have a good agreement with the effective masses of SiNWs along the [110] direction obtained through density-functional theory calculations[8] and experiments on optical properties of quantum wells.[9]

In the work presented here, bulk acoustic and optical phonons have been considered. In investigating hole transport in SiNWs, intersubband scattering is very important. This is because valence subbands are closely spaced in energy, and even at equilibrium higher energy subbands have a relatively high hole occupancy.[4] Neglecting intersubband scattering incorrectly yields very high mobility values, while our current theoretical model is insufficient to describe intersubband scattering from confined acoustic and optical phonons. Therefore we adopt bulk phonons, which are expected to become a better approximation with increase in nanowire diameter. We also mention that the use of bulk phonons physically corresponds to a case where the nanowire is surrounded by an acoustically similar material.[10]

Hole-phonon scattering rates are calculated using first-order perturbation theory and deformation potential approximation.[11] Scattering rates are numerically evaluated by using hole TB wave functions and a continuum model for phonons. While this can be a computationally intensive exercise, it provides a structure to investigate different SiNWs without resorting to simplifying assumptions for the band structures of individual SiNWs.

In performing EMC simulations, the SiNWs are considered to be long, undoped, and free of crystalline defects. A uniform electric field is assumed to be applied along the SiNW axis, and the temperature is assumed to be uniform throughout the SiNW. Holes with an equilibrium distribution are injected into the SiNW at time $t=0$. Standard EMC methodology and algorithms are used.[7,11] Up to the first five valence subbands are included for the SiNWs. Hole transport within each SiNW is limited to one-half of the one-dimensional Brillouin zone for that SiNW, and that region is divided into 4000 k-grid points (2000 points in the positive k

[a]Electronic mail: amit.verma@tamuk.edu.

 © 2009 American Institute of Physics

Downloaded 11 Jan 2010 to 128.95.215.143. Redistribution subject to AIP license or copyright; see http://jap.aip.org/jap/copyright.jsp

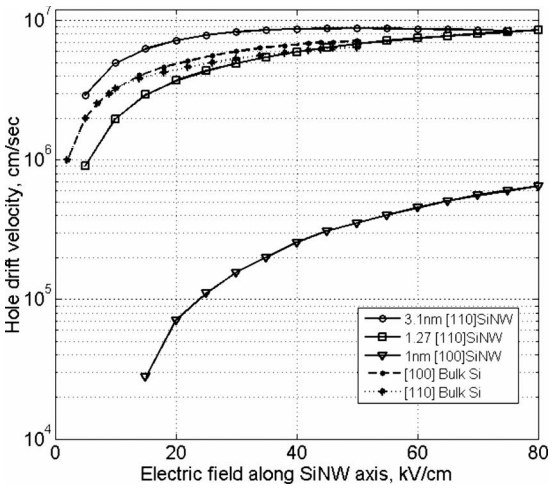


FIG. 1. Steady-state hole average drift velocity vs electric field at 300 K for 1.27 and 3.1 nm diameter [110] SiNWs and a 1 nm diameter [100] SiNW. Also included are results from bulk Si along [110] and [100] directions taken from Ref. 12.

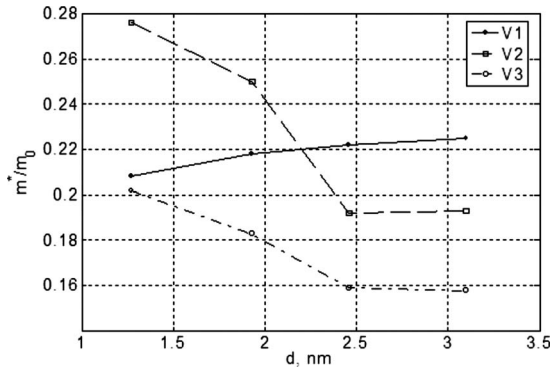


FIG. 2. Hole effective mass vs [110] SiNW diameter for the first three valence subbands. This figure is taken from Ref. 10.

direction and 2000 points in the negative k direction). Numerically tabulated values of the band structure, scattering rates, and possible final states after scattering are included in the simulation. In performing transient simulations, all holes are initially populated within the top valence subband, and the simulation is run for 15 000 iterations at zero electric field for holes to approach close to an equilibrium distribution.

III. RESULTS AND DISCUSSION

A. Steady state

Figure 1 shows the average steady-state hole drift velocity versus electric field at 300 K for 1.27 and 3.1 nm diameter [110] SiNWs and a 1 nm diameter [100] SiNW. Also included are previously reported hole drift velocity results for bulk Si along [110] and [100] directions for comparison.[12] The behavior for the three SiNWs and bulk Si is seen to be somewhat broadly similar, with some variations. For all the cases, the increase in average hole drift velocity is approximately linear at low electric fields, and then approaches saturation at relatively moderate to high electric fields. Additionally, for the 3.1 nm diameter [110] SiNW, the average hole velocity shows a slight negative differential mobility (NDM) behavior at relatively high electric fields. The difference in the hole velocity for the three SiNWs shown is attributed to the difference in hole effective mass and scattering rates.[4,10] Figure 2 depicts the hole effective masses versus diameter for the first three valence subbands for [110] SiNWs. As can be seen, the effective mass for the first valence subband shows relatively smaller change than the other two subbands, for which the effective masses decrease with increase in diameter. As will be discussed shortly, under both low-field and high-field conditions, all three subbands play a role in hole transport. This contributes partially to the increase in velocity (or mobility) with increase in diameter, seen in Fig. 1. In addition, Figs. 3(a)–3(c) show the phonon scattering rates for the 1.27 and 3.1 nm diameter [110] SiNWs and the 1 nm diameter [100] SiNW. Comparing the three scattering rates, we can clearly see that the [110] 3.1 nm diameter SiNW has the lowest phonon scattering rates, which further contributes to the higher hole velocity observed in Fig. 1. Concomitantly, the 1 nm diameter [100] SiNW is seen to have the highest scattering rate, which contributes to the lower velocity observed in Fig. 1. Using the prescription discussed shortly, room temperature hole low-field mobility for the 1 nm diameter [100] SiNW is evaluated to be 9.35 $cm^2/V\,s$. This is significantly lower than [110] SiNWs and bulk Si hole low-field mobility values, and comparable to the lower electron low-field mobility in these SiNWs.[4] This further illustrates the superior electronic response of the small diameter [110] SiNWs.

The saturation in velocity may be understood from Figs. 3 and 4. For simplicity we focus on the 3.1 nm diameter [110] SiNW, but the analysis applies to all the SiNWs considered in this work. Figure 3(b) depicts total hole acoustic and optical phonon scattering rates for the top valence subband for the 3.1 nm diameter [110] SiNW, where the deformation potentials for acoustic and optical phonon scattering are taken to be 5 eV and 13.24 eV/cm, respectively.[13] As can be seen from the figure, there is a significant enhancement in optical phonon scattering starting from $k \sim 6.5 \times 10^6/cm$. The observed optical phonon scattering peaks are associated with the onset of optical phonon emission and result in hole transition to the top of the first subband. This strong enhancement of optical phonon emission prevents holes from gaining larger velocities with an increase in electric field. This can be further seen in Fig. 4, which shows the percentage hole occupancy of individual subbands as a function of electric field. It is clear from Fig. 4 that hole occupancy does not show any significant change over the range of electric fields considered. The role of optical phonon scattering in causing velocity saturation may also be gauged from the inset of Fig. 4, which shows total steady-state hole distribution at different electric fields. It can be seen from the figure that hole distribution shows only a relatively small change at higher electric fields.

Figure 5 depicts the average hole drift velocity versus electric field for a 1.27 nm diameter [110] SiNW at various temperatures. Drift velocity at high electric fields is again seen to saturate at all temperatures considered because of optical phonon emission. A reduction in temperature is also

Downloaded 11 Jan 2010 to 128.95.215.143. Redistribution subject to AIP license or copyright; see http://jap.aip.org/jap/copyright.jsp

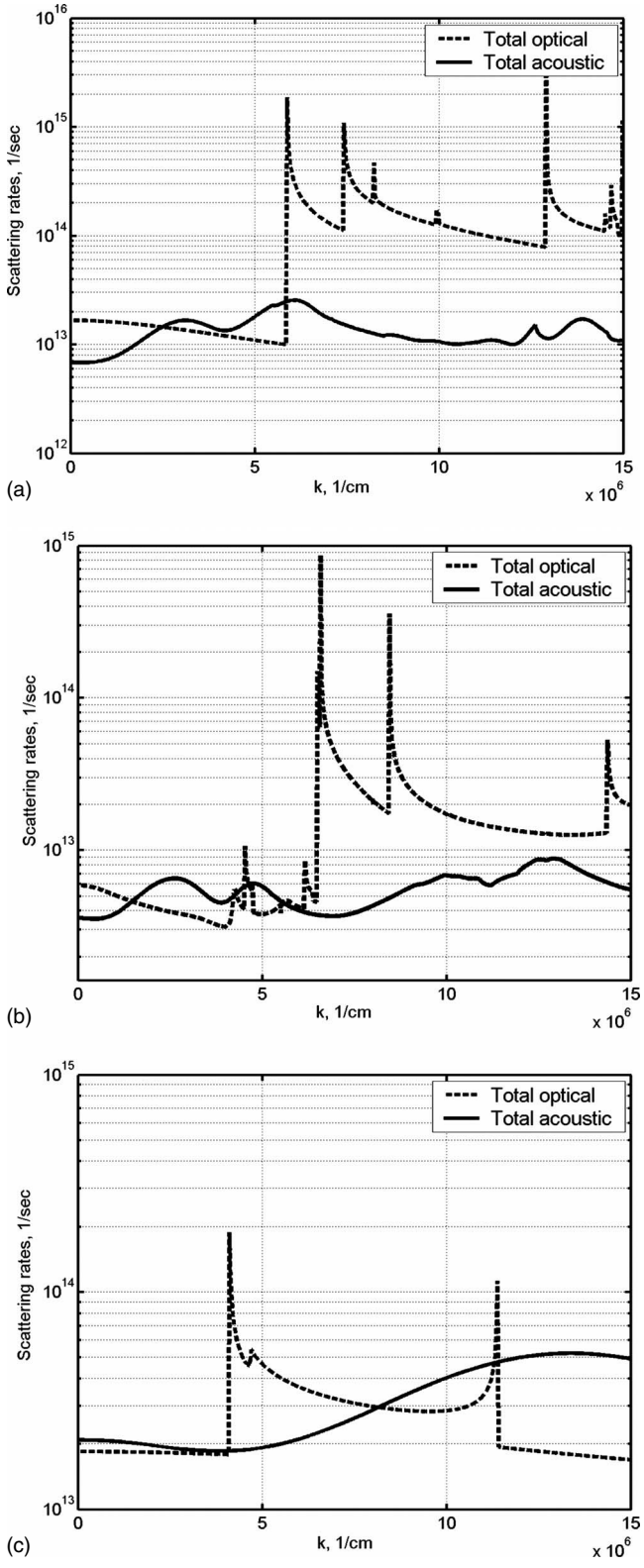


FIG. 3. First valence subband total hole acoustic and optical phonon scattering rates vs crystal momentum along the axis for (a) 1.27 nm diameter [110] SiNW, (b) 3.1 nm diameter [110] SiNW, and (c) 1 nm diameter [100] SiNW at 300 K.

seen to result in an expected increase in average drift velocity because of a decrease in phonon scattering rates.

While hole average drift velocity saturation is seen to be a common feature in all the SiNWs considered, the 3.1 nm diameter [110] SiNW also shows a small NDM at relatively

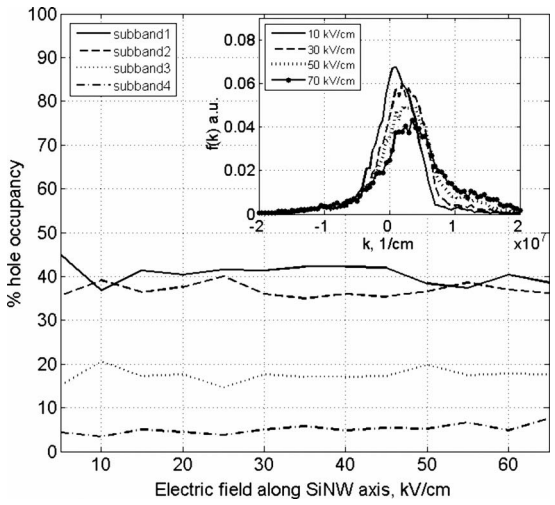


FIG. 4. Steady-state percentage hole occupancy of valence subbands vs electric field for a 3.1 nm diameter [110] SiNW at 300 K. Inset: Steady-state total hole distribution at different electric fields for a 3.1 nm diameter [110] SiNW at 300 K.

high electric fields. This phenomenon is attributed to nonparabolic subbands, where charge carriers reach regions within a subband where effective mass increases, and has also been suggested for carbon nanotubes.[14] As can be seen in Fig. 6, which depicts the first few valence subbands for the 3.1 nm diameter [110] SiNW, this region responsible for the hole NDM behavior occurs around $k \sim 5.5-6 \times 10^6/\mathrm{cm}$. As seen in Fig. 3(b), this is also close to the region where optical phonon scattering becomes dominant, which prevents a stronger NDM behavior. The overall role of scattering in preventing stronger NDM can be further gauged from Fig. 7, which shows the room temperature hole average drift velocity versus electric field with and without subbands 3 and 4 for the 3.1 nm diameter [110] SiNW. As can be seen from the figure, NDM is strongest for the case when we consider only subbands 1 and 2. The addition of more subbands increases the scattering rates, causing a greater relaxation of hole energy and preventing those holes from reaching regions within the subbands where effective mass increases. Other SiNWs discussed in Fig. 1 do not show a NDM behavior in the electric fields considered because their lower mobility pre-

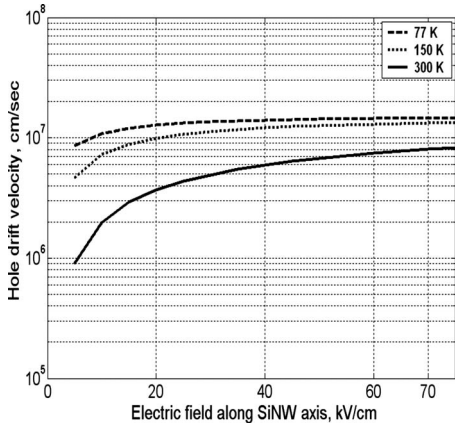


FIG. 5. Steady-state hole average drift velocity vs electric field at three different temperatures for a 1.27 nm diameter [110] SiNW.

Downloaded 11 Jan 2010 to 128.95.215.143. Redistribution subject to AIP license or copyright; see http://jap.aip.org/jap/copyright.jsp

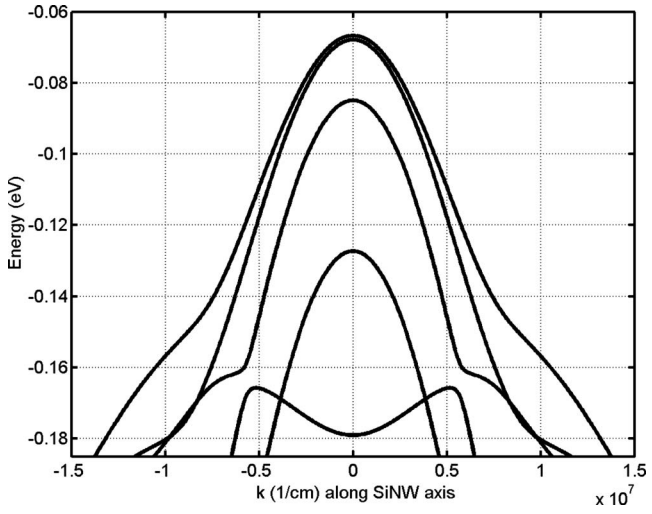


FIG. 6. First few valence subbands for the 3.1 nm diameter [110] SiNW. The top four subbands are included for the calculation results in this work.

vents holes from gaining enough crystal momentum to reach regions in their respective band structure where nonparabolicity becomes influential.

By incorporating the nonparabolicity of the subbands in mobility calculations, we also evaluate the carrier low-field hole mobility of SiNWs using

$$\mu_i = \frac{e}{k_B T} \frac{\int_{1\text{st BZ}} v_i^2(k_z) W_i(k_z)^{-1} f_0(k_z) dk_z}{\int_{1\text{st BZ}} f_0(k_z) dk_z} \quad (1)$$

and compare the results to the Monte Carlo values. In the above equation i is the subband index, and the scattering rates are $W_i(k_z) = \Sigma_\nu W_{i,\nu}(k_z)$ and $f_0(k_z) \approx e^{-E_i/k_B T}$. E_i is the hole energy in subband i, measured with respect to the highest valence subband and $v_i(k_z) = (1/\hbar)(dE_i/dk_z)$. Table I depicts the room temperature low-field hole and electron mobility for different [110] SiNWs using Eq. (1). It is important to point out that contrary to earlier results,[4] more accurate calculations here make low-field hole mobility for the 3.1 nm diameter [110] SiNW smaller than acoustic phonon limited electron mobility at room temperature. While only the 3.1 nm diameter SiNW shows a relatively significant change in low-field mobility, this does illustrate the importance of including nonparabolic effects in calculations involving SiNW band structure.

TABLE I. Room temperature low-field electron and hole mobility (in $cm^2/V\,s$) calculated using Eq. (1) for different [110] SiNWs.

SiNW diameter (nm)	Hole mobility	Electron mobility
1.27	221	309
1.93	309	574
2.40	865	834
3.10	665	1037

B. Transient

Figure 8 depicts the evolution of the transient average hole drift velocity for a 3.1 nm diameter [110] SiNW for thermally injected holes at room temperature and at various electric fields. As can be seen, the behavior of hole velocity is somewhat different than the predicted behavior of charge carriers within carbon nanotubes,[15] where oscillations in the velocity due to the streaming motion of charge carriers have been predicted.[16] The lack of oscillations in the hole velocity is primarily attributed to significant damping due to phonon scattering. The relative influence of acoustic phonon scattering in causing damping may be gauged from the inset of Fig. 8, which shows the evolution of the drift velocity of thermally injected holes in a 3.1 nm diameter [110] SiNW without acoustic phonon scattering. As can be seen, the absence of acoustic phonon scattering results in the appearance of a few clear oscillations, which disappear after approximately

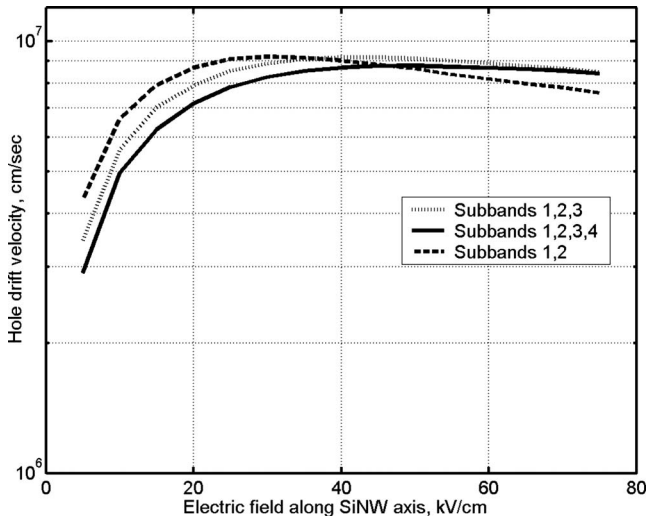


FIG. 7. Steady-state hole average drift velocity vs electric field at 300 K for a 3.1 nm diameter [110] SiNW with and without subbands 3 and 4. Inclusion of more subbands increases the scattering rates and decreases the magnitude of the observed NDM.

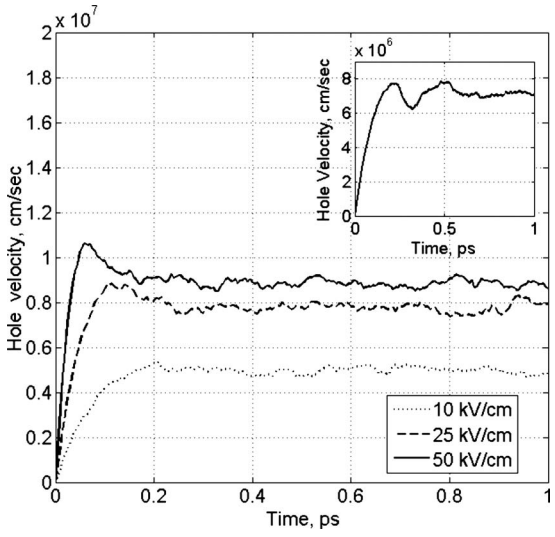


FIG. 8. Evolution of average hole velocity vs time for a 3.1 nm diameter [110] SiNW for different electric fields at 300 K. Inset: Evolution of average hole velocity vs time for a 3.1 nm diameter [110] SiNW at 10 kV/cm without acoustic phonon scattering at 300 K.

Downloaded 11 Jan 2010 to 128.95.215.143. Redistribution subject to AIP license or copyright; see http://jap.aip.org/jap/copyright.jsp

0.5 ps primarily because of intersubband and optical phonon absorption scattering. The other SiNWs considered here show a similar behavior. We also find the hole mean free path for a thermally injected hole at room temperature for the small diameter SiNWs considered in this work ([110] axially aligned 1.27 and 3.1 nm diameters and [100] axially aligned 1 nm diameter) to be less than 10 nm at various electric fields.

IV. CONCLUSIONS

In conclusion high-field hole transport in small diameter SiNWs has been modeled using EMC simulations. It is found that at relatively moderate to high electric fields, hole velocity in these dimensionally reduced structures saturates due to high optical phonon emission scattering above a crystal momentum threshold. A small NDM is observed for the large diameter SiNW. Since hole occupancy in various subbands shows only a minor change from the equilibrium value due to the high scattering rates above the threshold, this small NDM is attributed to holes reaching regions of the subbands where effective mass increases. Transient simulations for the hole transport show an absence of velocity oscillations due to the streaming motion of holes due to significant acoustic, optical phonon absorption, and intersubband scattering. Transient simulations also show that the mean free path for holes injected at room temperature is less than 10 nm for different electric fields considered.

ACKNOWLEDGMENTS

The authors acknowledge the use of High Performance Computing resource at the Texas A&M University-Kingsville supported through NSF Grant No. NSF-0619810. They are grateful to the National Institute of Standards and Technology for supporting this work.

[1] N. Singh, A. Agarwal, L. K. Bera, T. Y. Liow, R. Yang, S. C. Rustagi, C. H. Tung, R. Kumar, G. Q. Lo, N. Balasubramanian, and D.-L. Kwong, IEEE Electron Device Lett. **27**, 383 (2006).
[2] J. Hahm and C. M. Lieber, Nano Lett. **4**, 51 (2004).
[3] C. R. Leao, A. Fazzio, and J. R. Silva, Nano Lett. **7**, 1172 (2007).
[4] A. K. Buin, A. Verma, and M. P. Anantram, J. Appl. Phys. **104**, 053716 (2008).
[5] Y. Cui, Z. Zhong, D. Wang, W. U. Wang, and C. M. Lieber, Nano Lett. **3**, 149 (2003).
[6] A. Verma, A. K. Buin, M. P. Anantram, and R. Nekovei, Proceedings of the IEEE Eighth International Conference on Nanotechnology, Arlington, TX, 2008 , pp. 374–376.
[7] *Monte Carlo Device Simulation: Full Band and Beyond*, edited by K. Hess (Kluwer Academic, Dordrecht, 1991).
[8] T. Vo, A. J. Williamson, and G. Galli, Phys. Rev. B **74**, 045116 (2006).
[9] M. Virgillo and G. Grosso, J. Appl. Phys. **100**, 093506 (2006).
[10] A. K. Buin, A. Verma, A. Svizhenko, and M. P. Anantram, Nano Lett. **8**, 760 (2008).
[11] C. Jacoboni and P. Lugli, *The Monte Carlo Method for Semiconductor Device Simulation* (Springer, Wien, 1989).
[12] G. Ottaviani, L. Reggiani, C. Canali, F. Nava, and A. Alberigi-Quaranta, Phys. Rev. B **12**, 3318 (1975).
[13] M. V. Fischetti and S. E. Laux, J. Appl. Phys. **80**, 2234 (1996).
[14] V. Perebeinos, J. Tersoff, and P. Avouris, Nano Lett. **6**, 205 (2006).
[15] A. Verma, M. Z. Kauser, and P. P. Ruden, J. Appl. Phys. **97**, 114319 (2005).
[16] D. Jovanovic and J. P. Leburton, Superlattices Microstruct. **11**, 141 (1992).

Downloaded 11 Jan 2010 to 128.95.215.143. Redistribution subject to AIP license or copyright; see http://jap.aip.org/jap/copyright.jsp